ACS APPLIED MATERIALS & INTERFACES

Research Article

www.acsami.org

Open Access on 09/03/2015

# Improved in Vitro Blood Compatibility of Polycaprolactone Nanowire Surfaces

Victoria Leszczak[†] and Ketul C. Popat*[,†,‡]

[†]Department of Mechanical Engineering, [‡]School of Biomedical Engineering, Colorado State University, Fort Collins, Colorado 80523, United States

**ABSTRACT:** There are a multitude of polymeric materials currently utilized to prepare a variety of blood-contacting implantable medical devices. These devices include tissue grafts, coronary artery and vascular stents, and orthopedic implants. The thrombogenic nature of such materials can cause serious complications in patients, and ultimately lead to functional failure. To date, there is no truly hemocompatible biomaterial surface. Nanostructured surfaces improve cellular interactions but there is a limited amount of information regarding their blood compatibility. In this study, the in vitro blood compatibility of four different surfaces (control, PCL; nanowire, NW; collagen immobilized control, cPCL; collagen immobilized nanowire, cNW) were investigated for their use as interfaces for blood-contacting implants. The results presented here indicate enhanced in vitro blood compatibility of nanowire surfaces compared control surfaces. Although there were no significant differences in leukocyte adhesion, there was a decrease in platelet adhesion on NW surfaces. Scanning electron microscopy images showed a decrease in platelet/leukocyte complexes on cNW surfaces and no apparent complexes were formed on NW surfaces compared to PCL and cPCL surfaces. The increase in these complexes likely contributed to a higher expression of specific markers for platelet and leukocyte activation on PCL and cPCL surfaces. No significant differences were found in contact and complement activation on any surface. Further, thrombin antithrombin complexes were significantly reduced on NW surfaces. A significant increase in hemolysis and fibrinogen adsorption was identified on PCL surfaces likely caused by its hydrophobic surface. This work shows the improved blood-compatibility of nanostructured surfaces, identifying this specific nanoarchitecture as a potential interface for promoting the long-term success of blood-contacting biomaterials.

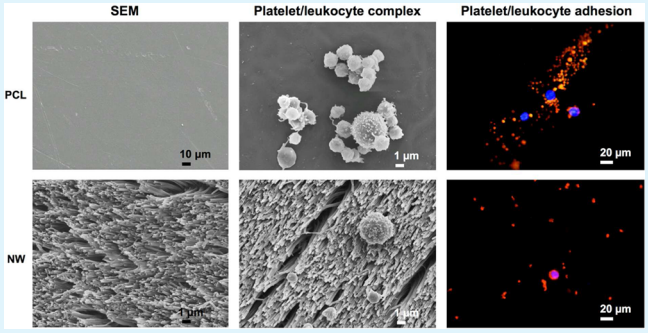


**KEYWORDS:** *polycaprolactone nanowire surfaces, hemocompatibility, platelet activation, leukocyte adhesion, hemolysis*

## INTRODUCTION

There are a multitude of polymeric materials such as ultrahigh molecular weight polyethylene,[1] polyether ether ketone,[2] and polycaprolactone,[3] currently utilized in several blood-contacting implantable medical devices such as tissue grafts,[4−6] coronary and vascular stents,[7] and orthopedic implants.[8] Despite how often these devices are used to treat tissue or organ failure, all these materials suffer from undesirable blood-material interactions. The thrombogenic nature of the material surface can cause serious complications in patients such as acute or chronic inflammation, fibrosis, infection, and/or thrombosis,[9,10] ultimately leading to implant failure.[11] Further, almost all short- and long-term implanted medical devices that come in contact with blood require a considerable amount of anticoagulation treatment, which comes with a high risk and a high cost to the patient.[12] Current research is focused on understanding the interaction of the blood and its components with material surfaces as well as developing surfaces that have toward favorable interactions with blood and its components.[13−15] The ability to regulate immune reactions on a material surface is vital for the success of any implantable biomedical device and also determines its hemocompatibility. To this day, there is no truly hemocompatible surface.[12] All blood-contacting materials have been shown to initiate an immunological response. Thus, improving the material surface compatibility with blood and its components could eliminate the need for intervention postimplantation.

When blood comes in contact with a material surface, an intricate series of highly interconnected events, such as platelet and leukocyte adhesion/activation and stimulation of complement and coagulation cascades, are initiated and controlled by the surface properties.[16] Key blood serum proteins, such as fibrinogen, adsorb and undergo conformational changes on the surface, thus mediating these events. Proteins can adsorb on the surface in different quantities, densities, conformations, and orientations, depending on the chemical and physical characteristics of the surface.[17] The layer of adsorbed proteins influences the adhesion and activation of platelets and leukocytes. Activated platelets express proteins such as platelet factor-4 (PF-4) and P-selectin, which, in turn, recruits leukocytes on the

Received: June 5, 2014
Accepted: September 3, 2014
Published: September 3, 2014

  

surface, facilitating the formation of platelet/leukocyte complexes. This further stimulates two pathways, better known as the intrinsic pathway (contact activation) and the extrinsic pathway (tissue factor), which may lead to thrombosis and/or a fibrous capsule. Both pathways involve activation of zymogens, eventually converging on a common pathway leading to clot development via formation of thrombin and fibrin.[18] Further, red blood cells may also get lysed when in contact with the surface, releasing adenosine diphosphate (ADP), which additionally promotes platelet aggregation on the material surface.[19] Thus, it is critical to evaluate and understand these events on material surfaces.

There are a variety of biochemical and topographical cues present naturally within human tissues that have favorable interactions with blood. Biomimetic surfaces have elicited promising cellular responses via biomolecular recognition, which can easily be regulated with changes to design parameters of the material surface.[20] Enhanced cellular responses to polymers surfaces modified with extracellular matrix (ECM) components, such as collagen I, are well documented. Collagen I is the main component in the ECM of blood vessels as well as other tissues in the body, making it an attractive molecule to modify the material surface. Studies with biofunctionalized collagen scaffolds have shown enhanced proliferation and differentiation of neural precursor cells,[21] improved bioactivity for bone engineering,[22,23] and increased endothelial cell organization and cell survival.[24] However, not much is known about the hemocompatibility of collagen immobilized surfaces.[25,26] Further, cells in vivo are constantly interacting with their surroundings that are composed of cues at a micro- and nanometer level.[27,28] Thus, by mimicking this environment in vitro, cell interaction with the surface can be controlled.[29−32] Nanostructured material surfaces have been shown to elicit appropriate cellular interactions with the biomaterial surface such as promotion of an osteoblast phenotype,[33,34] adhesion and alignment of smooth cells[35,36] and enhanced filopodia interactions with the environment.[37] Despite all these studies that suggest a correlation between nanoscale surface features and cell functionality, there is a limited amount of information in literature about the hemocompatibility of nanostructured surfaces.[38,39]

In this study, we have evaluated the ability of collagen-immobilized nanostructured surfaces as interfaces for blood-contacting materials. Nanowire surfaces were fabricated from polycaprolactone using a nanotemplating technique. Polycaprolactone is used in a multitude of FDA approved implants, drug delivery devices, sutures as well as adhesion barriers.[40,41] Previous studies have shown that polycaprolactone nanowire surfaces support reduced platelet adhesion and activation, and improve cellular functionality.[38,42] The nanowire surfaces were also immobilized with collagen, a protein abundantly found in the extracellular matrix of all tissues. Studies have shown enhanced cellular response to these surfaces as well.[42] Thus, in this study, the effect of the collagen immobilization on nanowire surfaces to blood and its components was investigated to better understand their effects on hemocompatibility. Fibrinogen binding from blood plasma to the surfaces after 2 h was investigated using an ELISA. The functionality of platelets and leukocytes were investigated on surfaces after 2 h of contact with whole blood plasma using a cell cytotoxicity assay, fluorescence microscopy and scanning electron microscopy (SEM). PF-4 release from activated platelets, SC5b-9 and thrombin antithrombin (TAT) complexes were quantified using ELISA. Contact activation was characterized via chromogenic analysis to determine the amount of kallikrein deposited on the surfaces. Further, a hemolytic assay was used to determine erythrocyte lysis. This work provides an in depth look at the hemocompatibility of collagen immobilized nanowire surfaces, utilizing a simple nanotemplating and collagen immobilization technique, which can lead to further development of these surfaces for blood-contacting implantable devices.

## METHODS AND MATERIALS

**Fabrication of Nanostructured Surfaces.** Control (PCL) surfaces were fabricated by sintering polycaprolactone pellets (MW = 80 000, Sigma) on a glass plate in a 10 mm Teflon washer. The resulting discs were then air-cooled cut using a 10 mm biopsy punch.

Polycaprolactone nanowire surfaces (NW) were fabricated using a solvent free nanotemplating technique with 20 nm diameter nanoporous aluminum oxide membranes.[43] PCL discs were positioned flat side down on the membrane surface and placed in an oven at 115 °C for 3−5 min, allowing the nanowires to gravimetrically extrude through the membrane. The aluminum oxide membranes were dissolved in 1 M NaOH for 75 min following the extrusion to release the nanowires. The surfaces were washed in DI water (3×), dried, and stored in a desiccator until their use was required.

Prior to any further use, all surfaces were sterilized in 70% ethanol for 30 min, followed by a phosphate buffered solution (PBS) rinse (2×). The surfaces were then air-dried and further sterilized by UV exposure for 30 min.

**Immobilization of Collagen on PCL and NW surfaces.** PCL and NW surfaces were immobilized with collagen in three subsequent steps.[44] First, the surfaces were subjected to aminolysis by incubation in 1,6-hexanediamine/2-propanol (6% w/v) for 10 min at 37 °C followed by rinsing with DI water (3×) to remove excess and unreacted 1,6-hexanediamine. Second, the surfaces were incubated in a gluteraldehyde (1 wt %) solution at 2−4 °C for 24 h and further rinsed with DI water (3×) to remove excess gluteraldehyde. Third, the surfaces were placed in a collagen solution (1% w/v) for 24 h at 2−4 °C. After the incubation, the surfaces were rinsed with 0.1 M acetic acid solution to remove unimmobilized collagen, followed by a DI water rinse (3×).

Notation for different surfaces in the rest of the paper is as follows: control (PCL), control + collagen (cPCL), nanowire (NW), and nanowire + collagen (cNW).

**Characterization of surfaces.** The surface architecture was characterized using scanning electron microscopy (SEM). Prior to imaging, surfaces were coated with 10 nm of gold. Surfaces were imaged at 7 kV and surface morphology was investigated to ensure similar architectures before and after collagen immobilization.

Surface wettability was characterized using a goniometer (ramé-hart Model 250 standard goniometer). One microliter of DI water was formed on the tip of the syringe and the syringe was lowered so that the droplet detached on the surface. Images were captured every 30 s for 5 min after contact of droplet with the surface by a camera leveled with the surface. Images were then analyzed with accompanying software (DROPimage advanced software) to measure contact angles. Each experiment was performed on three different locations and on at least three of each PCL, cPCL, NW, and cNW surface.

**Plasma Isolation from Whole Blood and Incubation on Different Surfaces.** Whole blood from a healthy individual was drawn into standard 10 mL ethylenediaminetetraacetic acid (EDTA) coated vacuum tubes using venipuncture by a phlebotomist. The protocol for blood isolation from healthy individuals was approved by Colorado State University Institutional Review Board. To account for the platelet plug and locally activated platelets resulting from the needle insertion, the first tube was discarded. The blood vials were centrifuged at 300*g* for 15 min to separate the plasma from the erythrocytes. The plasma was then pooled into fresh tubes and allowed to sit for 15 min prior to being used. The surfaces were incubated with

1 mL of pooled plasma in a 24-well plate at 37 °C and 5% $CO_2$ on a horizontal shaker plate (100 rpm) for 2 h.

**Cytotoxicity Assay.** The material cytotoxicity was characterized using a commercially available lactate dehydrogenase (LDH) cytotoxicity assay kit (Cayman Chemical). The protocol provided by the manufacturer was followed. In brief, the plasma-incubated surfaces were shaken on a horizontal shaker plate (1000 rpm) for 5 min at room temperature. The surface-exposed plasma samples as well as the standards were transferred to a 96-well plate. A reaction solution consisting of 96% v/v assay buffer, 1% v/v NAD+1%, v/v lactic acid, 1% v/v INT, and 1% v/v LDH diaphorase was added in equivalent amounts (1:1) to all standards and samples. This solution was incubated with gentle shaking on a horizontal shaker plate (100 rpm) for 30 min at room temperature. After the incubation, the absorbance of the solution was immediately measured at a wavelength of 490 nm to determine the cytotoxic effects of the different surfaces.

**Fibrinogen Binding from Plasma on Different Surfaces.** Fibrinogen binding from plasma on different surfaces was investigated using an enzyme-linked immunoassay (ELISA, GenWay). The protocol provided by the manufacturer was followed. In brief, diluted surface-exposed plasma samples (1:200 in assay diluent) and human fibrinogen antigen standards were transferred into a microassay well plate and incubated for 60 min at room temperature. The samples were removed and the wells were washed (4×) with the wash buffer and were incubated with enzyme antibody conjugate for 30 min at room temperature without exposure to light. The samples were removed and the wells were washed (4×) with the wash buffer and were incubated with tetramethylbenzidine buffer (TMB) solution for 10 min at room temperature in a dark environment. The reaction was stopped with stop solution and the optical density was immediately measured using a spectrophotometer at 450 nm.

**Platelet/Leukocyte Adhesion on Different Surfaces.** Cellular adhesion on different surfaces was investigated by fluorescence microscopy imaging using rhodamine phalloidin cytoskeleton stain and 4′6-diamidino-2-phenylindole dihydrochloride (DAPI). The unadhered cells were removed by aspirating the plasma from the surfaces followed by gently rinsing (2×) with PBS. The surfaces were then transferred to a new 24-well plate. Cells that adhered to the surfaces were fixed in 3.7 wt % formaldehyde in PBS for 15 min at room temperature and washed (3×, 5 min each) in PBS. The cell membranes were permeabilized using 1% Triton-X in PBS at room temperature for 3 min. The surfaces were then transferred to a new 24-well plate and incubated with 500 $\mu$L of rhodamine phalloidin solution in PBS for 25 min at room temperature. After 25 min, 0.2 $\mu$g/mL DAPI stain was added to each well. Following 5 min of incubation, the solution was aspirated and surfaces were rinsed with PBS and then imaged using a fluorescence microscope (Zeiss). Adherent leukocytes on 50× images were counted. All images were processed using ImageJ software.

**Platelet/Leukocyte Morphology on Different Surfaces.** The platelet−leukocyte morphology and interaction with the surfaces was investigated using SEM imaging. The unadhered cells were removed by aspirating the plasma from the surfaces followed by gently rinsing (2×) with PBS. The surfaces were then transferred to a glass Petri dish and the platelets and leukocytes that adhered were fixed by incubation in a solution of primary fixative (6% glutaraldehyde (Sigma), 0.1 M sodium cacodylate (Polysciences), and 0.1 M sucrose (Sigma)) for 45 min. The surfaces were then transferred to a secondary fixative (primary fixative without glutaraldehyde) for 10 min. The surfaces were then placed in consecutive solutions of ethanol (35%, 50%, 70%, and 100%) for 10 min each. For further dehydration, surfaces were placed into a solution of hexamethyldisilazane (HMDS, Sigma) for 10 min. The surfaces were then air-dried and stored in a desiccator until further imaging by SEM. Prior to imaging, the substrates were coated with a 10 nm layer of gold and imaged at 7 kV.

**Platelet/Leukocyte Detection on Different Surfaces by Immunofluorescence and Western Blotting.** Immunofluorescence staining and a western blotting technique were used to determine the cellular expression of proteins exclusive to platelets and leukocytes. The unadhered cells were removed by aspirating the plasma from the surfaces followed by gently rinsing (2×) with PBS. The surfaces were then transferred to a new 24-well plate and adherent cells were fixed in 3.7 wt % formaldehyde in PBS for 15 min at room temperature and washed (3×, 5 min each) in PBS. The cell membranes were permeabilized using 1% Triton-X in PBS at room temperature for 3 min, followed by washing with PBS (3×, 5 min each). The surfaces were then incubated in a blocking solution (10% bovine serum albumin (BSA) in PBS) for 30 min at room temperature. The surfaces were washed (3×, 5 min each) in PBS and incubated in primary antibodies specific to platelets and leukocytes, P-selectin and CD45, respectively (dilution 1:50, Santa Cruz Biotechnology) in a solution of 2% BSA in PBS for 1 h at room temperature. The surfaces were placed in new 24-well plates then washed (3×, 5 min each) in PBS, and incubated with fluorescently labeled secondary antibodies, donkey antigoat conjugated with Texas Red (for P-selectin) and chicken antimouse conjugated with fluorescein isothiocyanate (FITC) (for CD45) (dilution 1:100, Santa Cruz Biotechnology) in a solution of 2% BSA in PBS for 1 h at room temperature. The surfaces were washed (3×, 5 min each) in PBS and imaged with a fluorescence microscope (Zeiss). All images were processed using ImageJ software.

Western blotting was performed to partially quantify the expression of P-selectin and CD45. Briefly, the cells adhered on surfaces after 2 h of incubation in whole blood plasma were homogenized in radioimmunoprecipitation assay (RIPA) lysis buffer (10.0 mM Tris pH 7.4, 100.0 mM NaCl, 5.0 mM EDTA, 5.0 mM EGTA, 1.0% deoxycholate, 0.1% sodium dodecyl sulfate (SDS), 1.0% Triton X-100) containing protease inhibitor cocktail. The lysate was heated to 95 °C for 10 min in sample buffer (62.5 mM Tris−HCl pH 6.8, 10.0% glycerol, 5.0% $\beta$-mercaptoethanol, 2.0% SDS, 0.025% Bromophenol blue) in order to denature the proteins before gel loading. The protein extract was electrophoresed through 8% Tris−SDS gels and transferred to polyvinylidene fluoride (PVDF) membranes in 7.5% methanol. The blots were then blocked for 1 h at room temperature in a 10% BSA solution. Primary antibodies for P-selectin and CD45 were diluted 1:500 in 3% BSA in PBS−tween solution and incubated overnight at 4 °C. The blots were then washed with a PBS−tween solution (3×, 5 min each) before they were incubated with goat antimouse or donkey antigoat horseradish peroxidase (HRP) conjugated secondary antibodies (Santa Cruz Biotechnology) at a dilution of 1:5000 for 1 h at room temperature. The blots were then washed with PBS−tween solution (3×, 5 min each) followed by the detection of proteins using chemiluminescence (WestPico Chemiluminescent Substrate, Pierce). The blots were imaged using an Alpha Innotech FluorChem gel documentation system, and band intensities were analyzed using ImageJ software.

**PF-4 Expression on Different Surfaces.** PF-4 expression was measuresd using a commercially available enzyme linked immunosorbant assay kit (ELISA, RayBio) to evaluate platelet activation on different surfaces. The protocol provided by the manufacturer was followed. In brief, diluted substrate-exposed plasma samples (1:200 in assay diluent) and PF-4 standards were transferred into a microassay well plate and incubated for 2.5 h on a horizontal shaker plate (100 rpm) at room temperature. The wells were washed (4×) with wash buffer, and incubated with biotinylated antibody for 1 h on a horizontal shaker plate (100 rpm) at room temperature. The wells were then washed (4×) to remove unbound biotinylated antibody. This was followed by incubating the wells with a horseradish peroxidase (HRP)−streptavidin solution (1:25 000 in assay diluent) and incubated for 45 min on a horizontal shaker plate (100 rpm) at room temperature. Wells were then washed (4×) with the wash buffer. The TMB solution was then immediately added to each well and incubated for 30 min on a horizontal shaker plate (100 rpm) at room temperature with no exposure to light. The reaction was stopped with a stop solution and the optical density of the resulting solution was measured immediately thereafter at 450 nm to determine the amount of PF-4 released by platelets on each of the substrates.

**Contact Activation on Different Surfaces.** To investigate contact activation on different surfaces, the degree of plasma kallikrein expression (Chromogenix) present on surface-exposed plasma was evaluated with an acid stop method. The protocol provided by the

manufacturer was followed. In brief, the surface-exposed plasma samples were diluted 10-fold in Tris buffer (pH 7.8). 100 $\mu$L of each diluted surface-exposed plasma sample was placed in a 96-well plate and incubated at 37 °C and 5%$CO_2$ for 3−4 min. 100 $\mu$L of prewarmed (37 °C) substrate solution was added to all the samples and incubated at 37 °C and 5%$CO_2$ for 10 min. The reaction was stopped by 100 $\mu$L of 20% acetic acid to all samples. Plasma blanks were prepared by adding reagents in reverse order, without incubation. The optical density of samples was measured at 405 nm using a spectrophotometer to determine the degree of contact activation on the different surfaces.

**Complement Activation on Different Surfaces.** Complement activation was evaluated on different surfaces using an enzyme immunoassay (EIA, Quidel Corporation) to evaluate SC5b-9 complement activation. The protocol provided by the manufacturer was followed. In brief, microassay wells were rehydrated by incubating in a wash solution for 2 min at room temperature. The wash solution was aspirated and 100 $\mu$L of diluted surface-exposed plasma samples (1:10 in assay diluent), standards and controls were transferred into microassay wells and incubated for 60 min at room temperature. The wells were washed (5×) with wash buffer and incubated in SC5b-9 plus conjugate for 30 min at room temperature. Wells were then washed (5×) with wash buffer, followed by incubation in TMB solution for 15 min at room temperature without exposure to light. The reaction was stopped with stop solution and optical density was measured at 450 nm with a spectrophotometer to determine the amount of SC5b-9 complement activation present on the different surfaces.

**Thrombin Antithrombin (TAT) Complex Formation on Different Surfaces.** Thrombin antithrombin (TAT) concentration was measured using a thrombin antithrombin human ELISA kit (HemoScan). The protocol provided by the manufacturer was followed. In brief, a Nunc Maxisorp 96-well microtiter plate was coated with capture antibody in coating buffer overnight at 2−8 °C. The plate was washed (3×) with PBS−tween wash buffer. 100 $\mu$L of surface-exposed diluted plasma samples (1:200) along with standards were placed into the wells and incubated for 1 h at room temperature. The wells were washed (3×) before 100 $\mu$L of detection antibody solution was added and incubated at room temperature for 1 h. The wells were washed (3×) and 100 $\mu$L of substrate solution was added. After 20 min, the reaction was stopped with 50 $\mu$L of stop solution and optical density was read at 450 nm with a spectrophotometer.

**Thrombin Generation on Different Surfaces.** The rate of thrombin generation on different surfaces was calculated using a thrombin generation assay (TGA) (HemoScan). The protocol supplied by the manufacturer was followed. In brief, all surfaces were incubated in 350 $\mu$L diluted TGA plasma for 15 min. 175 $\mu$L of a prepared mixture of TGA reagent A and TGA reagent B was added to each vial. After 1 min, 10 $\mu$L of this mixture was placed into a vial containing 490 $\mu$L of buffer B. Vials were immediately placed back in the water bath after sampling. This was repeated after 2, 4, and 6 min for each sample and reference material. 150 $\mu$L of samples from each surface and standards were placed into a 96-well plate and incubated for 2 min at 37 °C and 5%$CO_2$. 50 $\mu$L of diluted substrate solution was added to each well and the covered well plate was incubated for 20 min at 37 °C and 5%$CO_2$. 50 $\mu$L of stop solution was added to each well and optical density was read immediately at 405 nm, using 540 nm as a reference wavelength. Thrombin generation rate was calculated by determining the highest rate between the two measured time points and correcting for the dilution factor (50×).

**Hemolytic Activity on Different Surfaces.** Hemolytic activity of different surfaces was investigated using a biomaterial hemolytic assay (HemoScan). The protocol supplied by the manufacturer was followed. In brief, cleaned surfaces along with reference materials were placed in syringes. One syringe without material was used as a negative control. An erythrocyte suspension (500 $\mu$L) was added to each syringe with specimen (test material, reference material or negative control). Air was removed and parafilm was used to close the outlet. Vials were incubated at 37 °C for 24 h while subjected to end-over end rotating. The erythrocyte suspension was carefully transferred to a centrifuge tube (1.5 mL) followed by centrifugation at high speed (3600$g$) for 1 min. Twenty microliters of supernatant from each sample or standard was placed into a 96-well plate along with 180 $\mu$L of assay buffer. The 96-well plate was mixed on a shaker plate before measuring optical density at 415 nm.

**Statistical Analysis.** Each qualitative experiment was performed on at least three different surfaces with at least three different whole blood plasma populations ($n_{min}$ = 9). All ELISA and EIA experiments were done on five surfaces. Further, all of the quantitative results were evaluated using one-way analysis of variance (ANOVA) with a Tukey's posthoc test. Statistical significance was considered at $p < 0.05$.

## RESULTS AND DISCUSSION

To this day, there is no truly hemocompatible surface that appropriately interacts with blood and its components.[12] All blood-contacting materials continue to induce unfavorable responses to whole blood and its components, such as protein adsorption, platelet and leukocyte adhesion/activation and stimulation of complement and coagulation cascades. These complications can potentially lead to implant failure and can limit the long-term success of blood-contacting devices. In this study, we have evaluated the effect of collagen immobilization to nanowire surfaces on blood and its components to better understand their effects on hemocompatibility. Improving the material surface compatibility with blood and its components could eliminate the need for intervention postimplantation. Our previous study has shown that polycaprolactone NW surfaces have superior hemocompatibility properties compared to nanofiber surfaces and hence were chosen for this study for further characterization.

SEM was used to characterize the different surfaces before and after the collagen immobilization process. Results indicate that before and after collagen immobilization, the surface architecture remains consistent without any significant changes (Figure 1). Previous studies have analyzed surface composition with X-ray photoelectron spectroscopy to ensure successful immobilization of collagen (data not shown).[42]

The wettability of different surfaces was evaluated using a goniometer (ramé-hart Model 250 standard goniometer). Water contact angles were determined over a course of 5 min. Contact angle is defined as the angle between the liquid/solid interface.[43] The results indicate significantly different

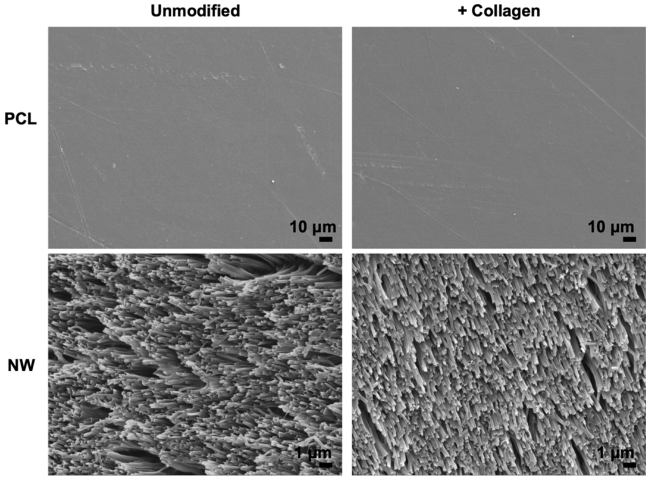


**Figure 1.** Representative SEM images of unmodified and collagen-immobilized PCL and NW surfaces. Results indicate similar nanostructured features before and after collagen immobilization.

contact angles between all four surfaces that were evaluated (Figure 2). PCL surfaces have the highest contact angle,

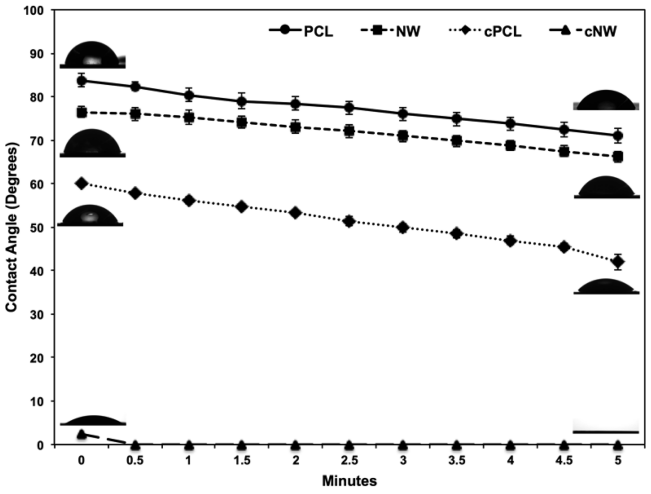


**Figure 2.** Contact angle measurements of PCL, NW, cPCL, and cNW surfaces taken every 30 s for 5 min. Results indicate significant differences in contact angles on all surfaces (PCL > NW > cPCL > cNW) ($p < 0.05$) at all time points (statistical symbols are not shown on the figure). Experiments were replicated with at least three different cell populations on at least three different samples ($n_{min} = 9$). Error bars represent standard error.

followed by NW and cPCL surfaces with cNW surfaces having the lowest contact angle. Further, the contact angles on all the surfaces decreased after 5 min of contact with water droplet. However, the contact angle on cNW surfaces dropped to zero within a few seconds of contact with the water droplet, indicating that the surface is extremely hydrophilic. Contact angles are dependent on surface area as well as specific surface properties such as polarity. The lower surface areas on PCL and cPCL surfaces attribute to the higher contact angles compared to those on NW and cNW surfaces. Further collagen coating the surfaces decreases contact angle due to an increase in polar groups immobilized to the surface. Surface wettability has been shown to have an influence on interactions between surfaces and blood proteins.[46,47]

The material cytotoxicity was investigated after 2 h of incubation in whole blood plasma using a commercially available lactate dehydrogenase (LDH) assay kit. LDH is a soluble enzyme located inside the cytoplasm of cells that is released upon loss of membrane integrity due to apoptosis or necrosis. Thus, this enzyme acts as a good marker of cell membrane integrity and can be used to evaluate the cytotoxic effects of the surfaces in this study. The results indicate all the surfaces demonstrate a comparable cytotoxicity on platelets/leukocytes (Figure 3). Thus, none of the surfaces possess short-term cytotoxic effects on the components of whole blood plasma. It is well-known that polycaprolactone is nontoxic and is also approved by the FDA for use in several implantable devices.[48] The results here indicate that topographical and biomolecular modifications to polycaprolactone do not significantly alter the cytotoxicity of the resulting surfaces.

Fibrinogen, produced by the liver, is present in blood plasma at a concentration of 200−400 mg/dL. Fibrinogen has two roles in the blood clotting cascade. It yields monomers that can polymerize into fibrin and is a cofactor in platelet aggregation. Prothrombin initiates the coagulation cascade when it is

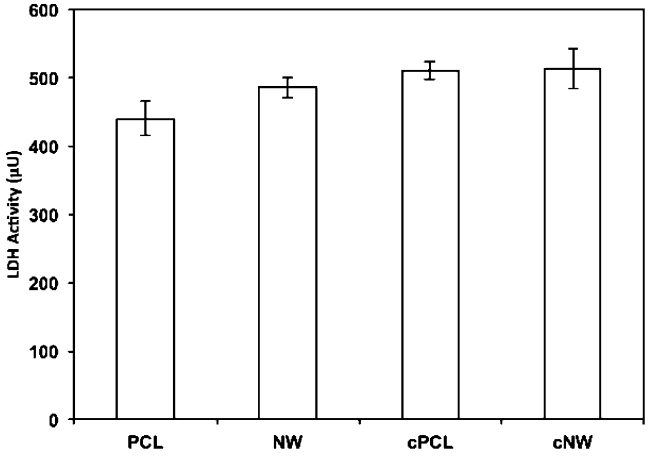


**Figure 3.** Cell cytotoxicity measured using an LDH assay on different surfaces after 2 h of incubation in whole blood plasma. The results indicate no significant difference in LDH activity on all the surfaces. Experiments were replicated with at least three different cell populations on at least three different samples ($n_{min} = 9$). Error bars represent standard error.

proteolytically cleaved to form thrombin. Thrombin then acts as a serine protease, which converts fibrinogen into fibrin. Under normal conditions, polymeric fibrin fibers form a thrombus network, also known as a blood clot. This clot can be characterized by the strength of the fibrin network that captures many components of blood. To evaluate the pro-coagulant activity, fibrinogen binding from blood plasma on different surfaces was evaluated after 2 h of incubation using commercially available human fibrinogen antigen assay. The plasma exposed to different surfaces was assayed to determine the amount of fibrinogen that was not bound on the material surface. The results indicate a significantly higher concentration of fibrinogen in the NW and cNW exposed whole blood plasma compare to that of PCL exposed whole blood plasma (Figure 4). This indicates significantly lower amount of fibrinogen binding on NW and cNW surfaces compared to PCL surfaces. Fibrinogen includes both hydrophobic and hydrophilic regions,

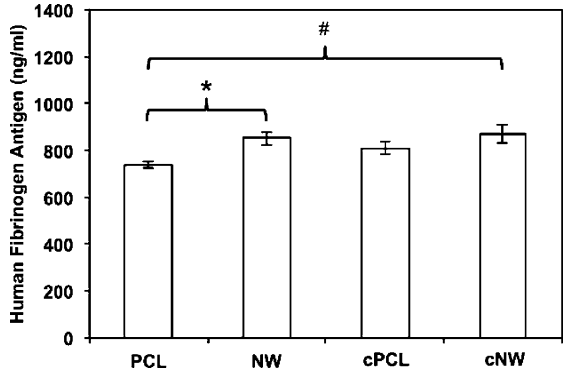


**Figure 4.** Human fibrinogen antigen concentration measured on surfaces after 2 h of incubation in whole blood plasma. The results indicate a significantly higher concentration of fibrinogen in the NW and cNW exposed whole blood plasma compare to that of PCL exposed whole blood plasma, indicating significantly lower amount of fibrinogen binding on NW and cNW surfaces compared to PCL surfaces (asterisk and pound symbols → $p < 0.05$). Experiments were replicated on 5 of each surface ($n_{min} = 5$). Error bars represent standard error.

giving it amphiphilic properties.[49] This allows it to bind on to a plethora of surfaces. However, blood plasma proteins have a higher affinity for binding unto uncharged hydrophobic surfaces as opposed to hydrophilic surfaces.[50,51] PCL surfaces are significantly more hydrophobic compared to NW and cNW surfaces, thus binding significantly more amount of fibrinogen compared to NW and cNW surfaces. However, the conformation and/or orientation of bound fibrinogen on the material surface plays a major role in determining its biocompatibility as well. It was found that platelet adhesion to biomaterial surfaces increases with increased coverage of fibrinogen only if the bound fibrinogen maintains a conformation so that its functional domain is recognizable by antibody probes.[52] The results from fibrinogen binding indicate that nanostructured surfaces may reduce fibrin clot formation, further promoting material hemocompatibility.

Cellular adhesion on different surfaces was investigated by fluorescence microscope imaging using rhodamine phalloidin cytoskeleton stain and DAPI nucleus stain to identify adherent platelets and leukocytes. Rhodamine phalloidin stained the cytoskeleton of both platelets and leukocytes. However, DAPI stained selectively for leukocytes as platelets are anuclear. The activated platelets can bind to each other as well as interact with leukocytes by binding to them, producing mixed aggregates. This platelet aggregation can be visualized using fluorescence microscopy. The results indicate lower cell adhesion and minimal platelet aggregation on NW surfaces as compared to PCL, cPCL, and cNW surfaces (Figure 5). Further, results also indicate higher cell adhesion on PCL surfaces followed by cNW and cPCL surfaces. However, there was minimal platelet aggregation observed on PCL surfaces as compared to cNW and cPCL surfaces. Upon platelet aggregation, microplatelet membrane particles are released, further promoting plasma coagulation.[53] Thus, the results indicate that NW surfaces may be less likely to promote plasma coagulation due to the lack of platelet aggregation.

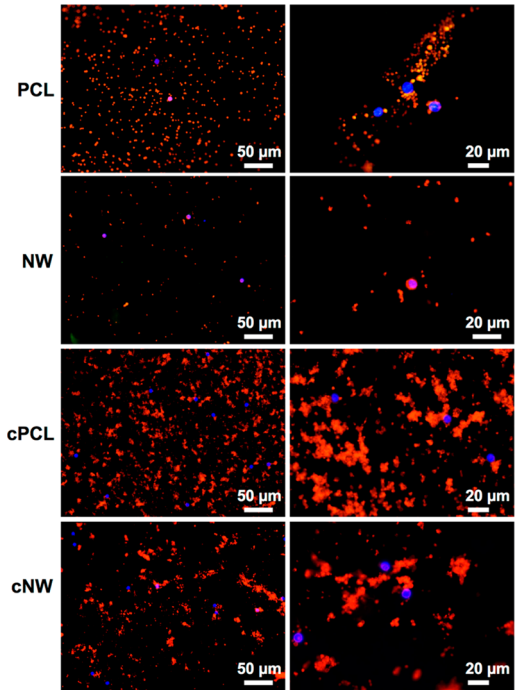


**Figure 5.** Representative fluorescence microscope images of adhered platelets and leukocytes stained with rhodamine-conjugated phalloidin (cytoskeleton) and DAPI (nucleus) on different surfaces after 2 h of incubation in whole blood plasma. The images indicate a decrease in cell adhesion and platelet aggregation on NW surfaces. Experiments were replicated with at least three different cell populations on at least three different samples ($n_{min}$ = 9).

Further, the fluorescence microscopy images were used to calculate the number of adhered leukocytes on different surfaces. The number of platelets could not be calculated due to higher degree of aggregation on the surfaces. The results indicate that there is no significant difference in leukocyte adhesion on the different surfaces (Figure 6).

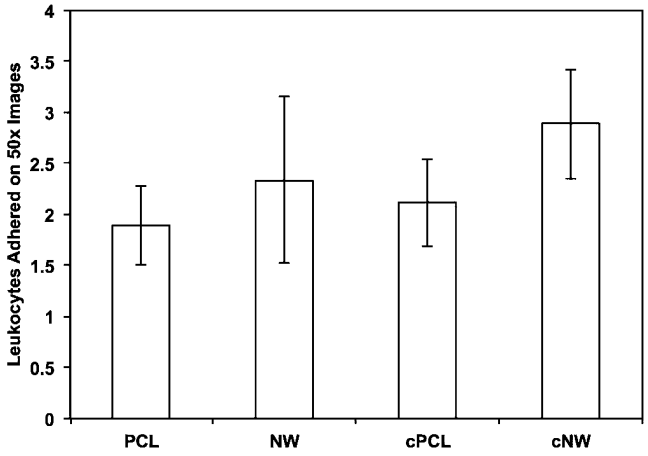


**Figure 6.** Adhered leukocytes after 2 h of incubation in whole blood plasma on different surfaces. No significant differences in leukocyte adhesion was seen on different surfaces. Experiments were replicated with at least three different cell populations on at least three different samples ($n_{min}$ = 9). Error bars represent standard error.

Platelet and leukocyte morphology, aggregation, and interaction on different surfaces were investigated using SEM imaging. The results indicate a decrease in platelet aggregation on NW surfaces as compared to PCL, cPCL, and cNW surfaces (Figure 7). High magnification SEM images reveal increased platelet aggregation on cPCL surfaces followed by PCL and cNW surfaces. Further, the SEM images also show no platelet/leukocyte interaction and complex formation on NW followed by minimal platelet/leukocyte interaction and complex formation on cNW surfaces. However, there is increased platelet/leukocyte interaction and complex formation on PCL and cPCL surfaces. Platelet/leukocyte interaction and complex formation appears to promote activation of platelets as evident by their altered morphology and dendritic extensions on PCL and cPCL surfaces. This platelet/leukocyte interaction is a reliable marker of a prothrombotic state and mixed aggregates are linked to several cardiovascular conditions.[54] Leukocytes may influence coagulation either directly, by producing procoagulant and anticoagulant molecules, or indirectly, by acting on vascular cells such as platelets, endothelial cells, and other leukocytes.[55] Studies have also shown that platelets–leukocyte interaction may also result in increased tissue factor (TF) expression, leading to fibrin deposition.[56] Thus, the results presented here indicate that NW surfaces may be more hemocompatible with lower probability for thrombogenic effects. The results also indicate that cNW surfaces may also reduce thrombogenic effects due to the decrease in platelet/leukocyte interaction and complex formation.

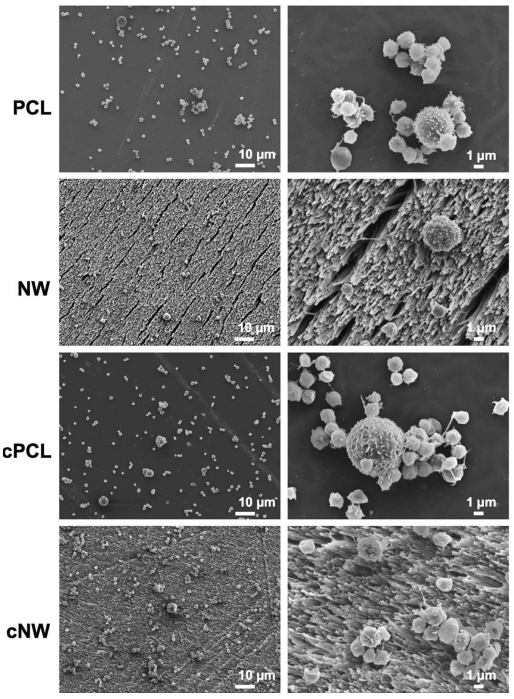


**Figure 7.** Representative SEM images of adhered platelets and leukocytes on different surfaces after 2 h of incubation in whole blood plasma. The surfaces were coated with a 10 nm layer of gold and imaged at 5−7 kV. Images show a lower degree of platelet/leukocyte interaction and cellular aggregation on NW surfaces. Experiments were replicated with at least three different cell populations on at least three different samples ($n_{min}$ = 9).

Platelet/leukocyte interaction and complex formation promotes further activation of platelets and leukocytes, advancing the coagulation cascade. Platelet and leukocyte activation was investigated after 2 h of incubation in whole blood plasma by immunofluorescence staining and a western blotting technique for specific marker proteins, P-selectin and CD45, that are known to be expressed in activated platelets and leukocytes, respectively. P-Selectin expression by platelets plays an essential role in the initial recruitment of leukocytes to the site of inflammation, further promoting fibrin deposition. It then promotes platelet aggregation via platelet−fibrin or platelet−platelet binding. CD45 is a transmembrane protein present on all human leukocytes and plays a role in signal transduction. CD45 has found to be not expressed by platelets. The results indicate a decrease in both P-selectin (TR-conjugated) and CD45 (FITC-conjugated) expression on NW and cNW surfaces compared to PCL and cPCL surfaces (Figure 8a). Further, a western blot technique was used to partially quantify the expression of P-selectin and CD45 on the surfaces. The results confirm the immunofluorescence images indicating a significant increase in P-selectin and CD45 expression on cPCL surfaces compared to PCL, NW, and cNW surfaces (Figure 8b). P-Selectin expression was also significantly higher on PCL surfaces compared to NW and cNW surfaces. Leukocytes adhere to the surface of an implanted biomaterial following platelet adhesion and activation in order to defend the body against foreign materials and this recruitment of leukocytes can cause further thrombogenic effects. Upon activation, leukocytes release granules, allowing them to easily adhere to collagen. Thus, increased adhesion and activation of platelets results in

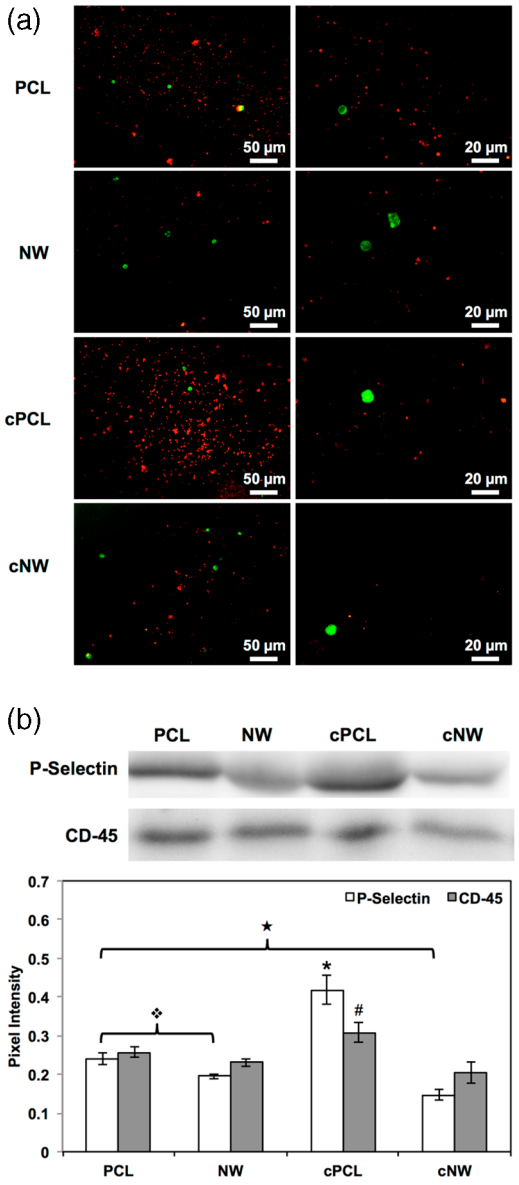


**Figure 8.** (a) Representative fluorescence microscope images of platelets immunostained for P-selectin and leukocytes immunostained for CD45 on different surfaces after 2 h of incubation in whole blood plasma. The images indicate a considerable reduction in P-selectin (TR-conjugated) and CD45 (FITC-conjugated) expression on NW and cNW surfaces compared to PCL and cPCL surfaces. Experiments were replicated with at least three different cell populations on at least three different samples ($n_{min}$ = 9). (b) Western blot analysis of P-selectin and CD45 expression on different surfaces after 2 h of incubation in whole blood plasma. Results indicate significant increase in P-selectin and CD45 expression on cPCL surfaces compared to PCL, NW, and cNW surfaces (asterisk and pound symbols → $p < 0.05$). P-Selectin expression was also significantly higher on PCL surfaces compared to NW and cNW surfaces (four-diamond and star symbols → $p < 0.05$). Experiments were replicated with at least three different cell populations on at least three different samples ($n_{min}$ = 9). Error bars represent standard error.

increased P-selectin expression on PCL and cPCL surfaces, which further promotes more leukocyte recruitment resulting in increased CD45 expression. Further, the cPCL surfaces provide signals to leukocytes, which further promotes their adhesion.

To further quantify platelet activation, the amount of PF-4 present in surface-exposed plasma samples was investigated. PF-4 is released from $\alpha$-granules in activated platelets during aggregation in a platelet release reaction. PF-4 is therefore an excellent indicator of platelet activation. A human PF-4 ELISA was used to quantify the amount of PF-4 released by activated platelets after 2 h of incubation in whole blood plasma. The results indicate a significant increase in PF-4 expression on cPCL surfaces compared to NW and cNW surfaces, and a significant decrease in PF-4 expression on NW surfaces compared to PCL and cPCL surfaces (Figure 9). Platelet

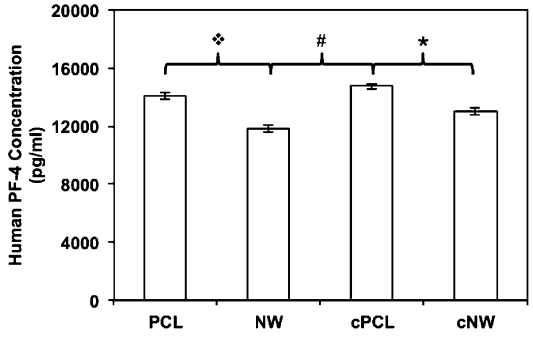


**Figure 9.** Platelet release reaction measured by the amount of PF-4 released from $\alpha$- granules within the platelets on different surfaces after 2 h of incubation in whole blood plasma. The results indicate a significant increase in PF-4 expression on cPCL surfaces compared to NW and cNW surfaces (asterisk and pound symbols $\rightarrow p < 0.05$) and a significant decrease in PF-4 expression on NW surfaces compared to PCL surfaces (four-diamond and star symbols $\rightarrow p < 0.05$). Experiments were replicated on 5 of each surface ($n_{min} = 5$). Error bars represent standard error.

activation and release of biomolecules such as PF-4 from activated platelets is influenced by the presence and interaction of leukocytes with platelets.[10] Further, the lower release of PF-4 from platelets after being exposed to NW and cNW surfaces may be due to the decrease in platelet/leukocyte interaction and complex formation (Figure 7).

Contact activation has been considered a significant cause for insufficient hemocompatibility of blood-contacting biomaterials because it is initiated by blood–biomaterial contact.[57] The proteins involved in the contact activation system, such as factors VII, IX, XI, XII, prekallikrein, and high molecular weight kininogen, have functions of being profibrinolytic, antiadhesive, anticoagulant, and pro-inflammatory.[58] The degree of contact activation on the different surfaces after 2 h of incubation in whole blood plasma was determined by measuring the activity of the kallikrein-a2-macroglobulin complex. Unlike factor XIIa, all kallikrein is released from the surface of the biomaterial. The results indicate no significant difference in contact activation on all the surfaces (Figure 10). This may be due to the fact that the surfaces have a similar surface charge since all surfaces are made from polycaprolactone.

The complement system, consisting of over 20 plasma proteins, such as C3 and C5, plays a significant role in the body's defense mechanisms against infection and "foreign" objects and supports the innate immune system.[16,59] Complement activation facilitates antibodies and phagocytic cells when clearing pathogens from an organism. The main functions are opsonization, chemotaxis, cell lysis, and aggregation of antigen-bearing agents. There are three pathways of complement activation, which converge to form the terminal complement

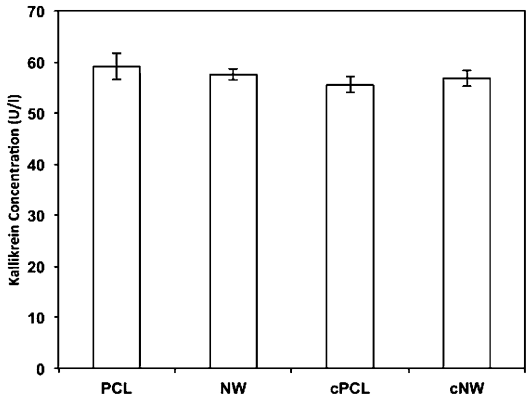


**Figure 10.** Contact activation measured by the amount of kallikrein on different surfaces after 2 h of incubation in whole plasma. The results indicate no significant difference in contact activation on the surfaces. Experiments were replicated on 5 of each surface ($n_{min} = 5$). Error bars represent standard error.

complex (TCC) or SC5b-9 complex.[60] The surface of an implant may activate an inflammatory reaction leading to the formation of the SC5b-9 complex. Therefore, quantifying this complex provides an accurate measurement of the degree of complement activation occurring in response to a material surface. In this study, a quantitative SC5b-9 EIA analysis was performed after surfaces were exposed to whole blood plasma for 2 h (Figure 11). The results indicate no significant

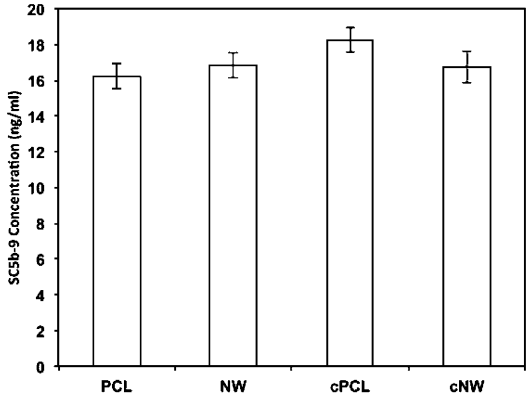


**Figure 11.** Complement activation measured by the amount of SC5b-9 activation on different surfaces after 2 h of incubation in human plasma. The results indicate no significant difference in the level of complement activation. Experiments were replicated on 5 of each surface ($n_{min} = 5$). Error bars represent standard error.

difference in SC5b-9 complex formation in response to the different surfaces indicating a similar inflammatory response. This indicates that altering the topography of PCL or immobilizing collagen does not significantly increase the activation of the complement system.

Thrombin, one of the key enzymes in the coagulation cascade, is known to promote the activation and aggregation of platelets. Thrombin also has a short half-life, making it difficult to determine its activity. Upon activation of the coagulation cascade, prothrombin is activated into thrombin. The primary inhibitor of thrombin is antithrombin and it forms a complex known as the thrombin antithrombin (TAT) complex. The TAT complex has been used as a marker for thrombin generation. The ability for the different surfaces to affect

intrinsic coagulation cascade turnover for thrombin generation was investigated with a TAT ELISA. The results indicate a significant decrease in TAT concentration on NW surfaces compared to PCL, cPCL and cNW surfaces, and an significant increase in TAT concentration on cPCL surfaces compared to PCL, NW and cNW surfaces (Figure 12). These results are in agreement with platelet activation results (Figures 8 and 9). Thrombin generation ultimately leads to platelet activation, and an increase in platelet activation was observed on cPCL surfaces, whereas there was a decrease in platelet activation was observed on NW surfaces.

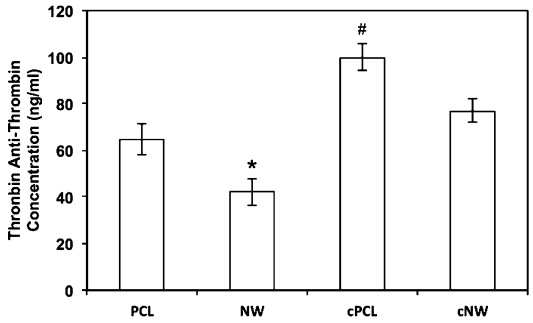


**Figure 12.** TAT concentration determined after 2 h of incubation of different surfaces in whole blood plasma. Results indicate a significant decrease in TAT concentration on NW surfaces compared to PCL, cPCL and cNW surfaces (asterisk symbol → $p < 0.05$) and an increase in TAT concentration on cPCL surfaces compared to PCL, NW and cNW surfaces (pound symbol → $p < 0.05$). Experiments were replicated on 5 of each surface ($n_{min} = 5$). Error bars represent standard error.

Further, the rate of thrombin generation on different surfaces was calculated using a thrombin generation assay (TGA). Thrombin promotes platelet activation and aggregation and is one of the key enzymes in the coagulation cascade. Thrombin has a short half-life, which makes it difficult to accurately determine its activity. Results indicate that thrombin generation rate was greatest on cNW surfaces over a period of 6 min, followed by cPCL surfaces, with NW surfaces having the lowest thrombin generation velocity (Figure 13). It is important to note that this assay was done over the course of 6 min whereas the previous assay determined the TAT complex formation after 2 h. These combined results indicate that the initial generation of thrombin is greatest on cNW surfaces; however, after 2 h, TAT complex formation is significantly higher on cPCL surfaces, indicating higher thrombin generation.

Hemolytic activity of different surfaces was investigated using a biomaterial hemolytic assay. Hemolytic activity is required to be tested for any blood-contacting medical device. The assay is centered on erythrocyte lysis, which can be induced by a variety of reasons such as contact, leachables, toxins, metal ions, surface charge or any other cause of erythrocyte lysis. The membranes of red blood cells undergo dynamic stress when exposed to a biomaterial and are considered fragile. The assay measures release of hemoglobin spectrophotometrically. The results indicate a significant increase in the amount of hemoglobin released on PCL surfaces, indicating more hemolysis compared to NW, cPCL, and cNW surfaces (Figure 14). This is undesirable because erythrocytes contain adenosine diphosphate (ADP), which is released when they are lysed, resulting in further platelet aggregation.[19] Studies have shown that material surfaces with the high contact angles and high work of adhesion cause more lysis of erythrocytes.[61] PCL surfaces have the highest contact angles compared to cPCL, NW, and cNW surfaces, which may be why significantly more erythrocyte lysis is caused by the PCL surfaces. However, there are no significant

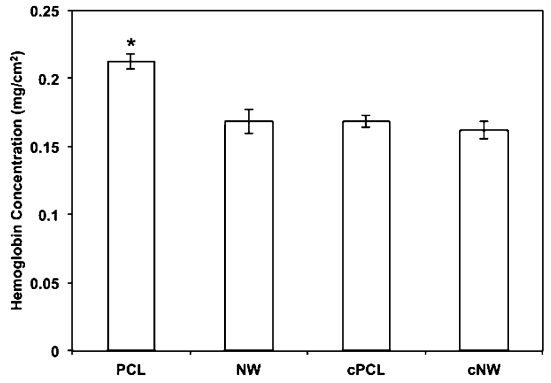


**Figure 14.** Hemoglobin release from an erythrocyte suspension was measured with a spectrophotometer after an incubation period of 24 h. Results indicate a significant increase in the amount of hemoglobin released on PCL surfaces compared to NW, cPCL, and cNW surfaces. Experiments were replicated on 5 of each surface ($n_{min} = 5$). Error bars represent standard error.

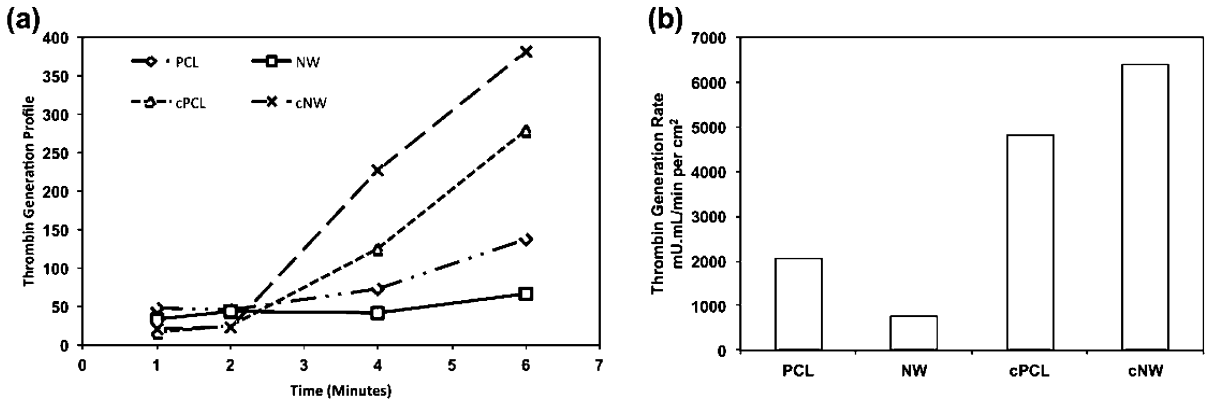


**Figure 13.** (a) Thrombin generation profile was measured with a spectrophotometer after 1, 2, 4, and 6 min. (b) Thrombin generation velocity was calculated as the largest difference between two points and normalized to area of each surface. No statistics were done, as this experiment was only performed once.

differences between NW and cNW surfaces, even though there are significant differences between their contact angles. This may be due to the fact that the topography is playing a dominant role on erythrocyte lysis compared to collagen modification.

## CONCLUSION

The thrombogenic effects of four different surfaces (PCL, NW, cPCL, cNW) were investigated for their use as interfaces for blood-contacting implants. The clotting cascade consists of many pathways that eventually converge to a common pathway and lead to the formation of a blood clot. It is important to understand how each components of the clotting cascade will interact with a biomaterial surface in order to be able understand the events that happen when a biomaterial comes in contact with blood. Results from our previous study suggest NW surfaces have superior hemocompatibility properties compared to electrospun polycaprolactone nanofiber surfaces and hence were chosen for this study. The results presented here indicate a decrease in the thrombogenic effects on NW surfaces compared to PCL, cPCL, and cNW surfaces. Proteins, such as fibrinogen and thrombin, as well as molecules released from platelets and leukocytes, and collagen, are known to be potent platelet activators.[16] Results from the studies presented here indicate that surfaces coated with collagen did not promote fully activated platelets alone but did promote more platelet aggregation. Although there were no significant differences in leukocyte adhesion on all the surfaces, there was a decrease in platelet adhesion on NW surfaces. SEM images showed a decrease in platelet/leukocyte complexes on cNW surfaces and no apparent complexes were formed on NW surfaces compared to PCL and cPCL surfaces, indicating that the nanowire topography may interrupt the interaction between platelets, and platelets/leukocytes. The increase in these complexes likely contributed to a higher expression of specific markers for platelet and leukocyte activation on PCL and cPCL surfaces. No significant differences were found in contact and complement activation. Further, thrombin antithrombin complexes were significantly reduced on NW surfaces. A significant increase in hemolysis and fibrinogen adsorption was identified on PCL surfaces, likely caused by its hydrophobic surface. Further studies are now directed toward more in depth understanding of the mechanisms underlying the enhanced hemocompatibility of nanostructured surfaces by investigating the effect of nanowire size, and evaluating in vivo response to nanostructured surfaces.

## AUTHOR INFORMATION

### Corresponding Author

*K. C. Popat. Tel: +1-970-491-1468. E-mail: ketul.popat@colostate.edu.

### Author Contributions

The paper was written through contributions of all authors. All authors have given approval to the final version of the paper.

### Funding

Research reported in this publication was supported by the National Institute of Arthritis and Musculoskeletal and Skin Diseases of the National Institutes of Health under Award Number 5-R21-AR057341-02. The content is solely the responsibility of the authors and does not necessarily represent the official views of the National Institutes of Health.

### Notes

The authors declare no competing financial interest.

## ABBREVIATIONS

(ADP) = adenosine diphosphate
(BSA) = bovine serum albumin
(cNW) = collagen immobilized NW
(cPCL) = collagen immobilized PCL
(DAPI) = 4′6-diamidino-2-phenylindole dihydrochloride
(ECM) = extracellular matrix
(EDTA) = ethylenediaminetetraacetic acid
(EGTA) = ethylene glycol tetraacetic acid
(EIA) = enzyme immunoassay
(ELISA) = enzyme-linked immune assay
(HMDS) = hexamethyldisilazane
(LDH) = lactate dehydrogenase
(NW) = nanowire
(PBS) = phosphate buffer solution
(PCL) = polycaprolactone
(SDS) = sodium dodecyl sulfate
(SEM) = scanning electron microscopy
(TAT) = thrombin antithrombin
(TGA) = platelet factor-4 (PF-4), thrombin generation assay
(TMB) = tetramethylbenzidine buffer

## REFERENCES

(1) Pruitt, L.; Furmanski, J. Polymeric Biomaterials for Load-Bearing Medical Devices. *JOM* **2009**, *61*, 14−20.
(2) Kurtz, S. M.; Devine, J. N. Peek Biomaterials in Trauma, Orthopedic, and Spinal Implants. *Biomaterials* **2007**, *28*, 4845−4869.
(3) Low, S.; Ng, Y.; Yeo, T.; Chou, N. Use of Osteoplugtm Polycaprolactone Implants as Novel Burr-Hole Covers. *Singapore Med. J.* **2009**, *50*, 777−780.
(4) Ze, Z.; King, M. W.; Guidoin, R.; Therrien, M.; Pezolet, M.; Adnot, A.; Ukpabi, P.; Vantal, M. H. Morphological, Physical and Chemical Evaluation of the Vascugraft® Arterial Prosthesis: Comparison of a Novel Polyurethane Device with Other Microporous Structures. *Biomaterials* **1994**, *15*, 483−501.
(5) Venkatraman, S.; Boey, F.; Lao, L. L. Implanted Cardiovascular Polymers: Natural, Synthetic and Bio-Inspired. *Prog. Polym. Sci.* **2008**, *33*, 853−874.
(6) Puskas, J. E.; Chen, Y. Biomedical Application of Commercial Polymers and Novel Polyisobutylene-based Thermoplastic Elastomers for Soft Tissue Replacement. *Biomacromolecules* **2004**, *5*, 1141−1154.
(7) Li, G.; Liu, Y.; Lan, P.; Li, Y.; Li, Y. A Prospective Bifurcated Biomedical Stent with Seamless Woven Structure. *J. Text. Inst.* **2013**, *104*, 1017−1023.
(8) Middleton, J. C.; Tipton, A. J. Synthetic Biodegradable Polymers as Orthopedic Devices. *Biomaterials* **2000**, *21*, 2335−2346.
(9) Anderson, J. M.; Rodriguez, A.; Chang, D. T. Foreign Body Reaction to Biomaterials. *Semin. Immunol.* **2008**, *20*, 86−100.
(10) Gorbet, M. B.; Sefton, M. V. Biomaterial-Associated Thrombosis: Roles of Coagulation Factors, Complement, Platelets and Leukocytes. *Biomaterials* **2004**, *25*, 5681−5703.
(11) *Biomaterials Engineering and Devices: Human Applications*; Wise, D. L.; Trantolo, D. J.; Lewandrowski, K.-U.; Gresser, J. D.; Cattaneo, M. V.; Yaszemski, M. J., Eds.; Vol. *1*; Humana Press: New York, 2000; pp 1−344.
(12) Ratner, B. D. The Catastrophe Revisited: Blood Compatibility in the 21st Century. *Biomaterials* **2007**, *28*, 5144−5147.
(13) Sin, M.-C.; Sun, Y.-M.; Chang, Y. Zwitterionic-based Stainless Steel with Well-Defined Polysulfobetaine Brushes for General Bioadhesive Control. *ACS Appl. Mater. Interfaces* **2013**, *6*, 861−873.
(14) Hoshi, R. A.; Van Lith, R.; Jen, M. C.; Allen, J. B.; Lapidos, K. A.; Ameer, G. The Blood and Vascular Cell Compatibility of Heparin-Modified Eptfe Vascular Grafts. *Biomaterials* **2013**, *34*, 30−41.

(15) Mohan, C. C.; Chennazhi, K. P.; Menon, D. In Vitro Hemocompatibility and Vascular Endothelial Cell Functionality on Titania Nanostructures under Static and Dynamic Conditions for Improved Coronary Stenting Applications. *Acta Biomater.* **2013**, *9*, 9568−9577.
(16) Gorbet, M. B.; Sefton, M. V. Biomaterial-Associated Thrombosis: Roles of Coagulation Factors, Complement, Platelets and Leukocytes. *Biomaterials* **2004**, *25*, 5681−5703.
(17) Roach, P.; Farrar, D.; Perry, C. C. Interpretation of Protein Adsorption: Surface-Induced Conformational Changes. *J. Am. Chem. Soc.* **2005**, *127*, 8168−8173.
(18) Wang, X.; Wang, E.; Kavanagh, J. J.; Freedman, R. S. Ovarian Cancer, the Coagulation Pathway, and Inflammation. *J. Trans. Med.* **2005**, *3*, 25.
(19) Alkhamis, T. M.; Beissinger, R. L.; Chediak, J. R. Red Blood Cell Effect on Platelet Adhesion and Aggregation in Low-Stress Shear Flow. Myth or Fact? *Trans. - Am. Soc. Artif. Intern. Organs* **1988**, *34*, 868−873.
(20) Feng, Y.; Zhao, H.; Zhang, L.; Guo, J. Surface Modification of Biomaterials by Photochemical Immobilization and Photograft Polymerization to Improve Hemocompatibility. *Front. Chem. Eng. China* **2010**, *4*, 372−381.
(21) O'Connor, S. M.; Stenger, D. A.; Shaffer, K. M.; Maric, D.; Barker, J. L.; Ma, W. Primary Neural Precursor Cell Expansion, Differentiation and Cytosolic $Ca^{2+}$ Response in Three-Dimensional Collagen Gel. *J. Neurosci. Methods* **2000**, *102*, 187−195.
(22) He, F.; Li, J.; Ye, J. Improvement of Cell Response of the Poly(lactic-co-glycolic acid)/Calcium Phosphate Cement Composite Scaffold with Unidirectional Pore Structure by the Surface Immobilization of Collagen Via Plasma Treatment. *Colloids Surf., B* **2013**, *103*, 209−216.
(23) Kalaskar, D. M.; Demoustier-Champagne, S.; Dupont-Gillain, C. C. Interaction of Preosteoblasts with Surface-Immobilized Collagen-based Nanotubes. *Colloids Surf., B* **2013**, *111*, 134−141.
(24) Huang, N. F.; Okogbaa, J.; Lee, J. C.; Jha, A.; Zaitseva, T. S.; Paukshto, M. V.; Sun, J. S.; Punjya, N.; Fuller, G. G.; Cooke, J. P. The Modulation of Endothelial Cell Morphology, Function, and Survival Using Anisotropic Nanofibrillar Collagen Scaffolds. *Biomaterials* **2013**, *34*, 4038−4047.
(25) Liu, T.-Y.; Lin, W.-C.; Huang, L.-Y.; Chen, S.-Y.; Yang, M.-C. Hemocompatibility and Anaphylatoxin Formation of Protein-Immobilizing Polyacrylonitrile Hemodialysis Membrane. *Biomaterials* **2005**, *26*, 1437−1444.
(26) Solouk, A.; Cousins, B. G.; Mirzadeh, H.; Seifalian, A. M. Application of Plasma Surface Modification Techniques to Improve Hemocompatibility of Vascular Grafts: A Review. *Biotechnol. Appl. Biochem.* **2011**, *58*, 311−327.
(27) Lord, M. S.; Foss, M.; Besenbacher, F. Influence of Nanoscale Surface Topography on Protein Adsorption and Cellular Response. *Nano Today* **2010**, *5*, 66−78.
(28) Norman, J.; Desai, T. Methods for Fabrication of Nanoscale Topography for Tissue Engineering Scaffolds. *Ann. Biomed. Eng.* **2006**, *34*, 89−101.
(29) Abidian, M. R.; Corey, J. M.; Kipke, D. R.; Martin, D. C. Conducting-Polymer Nanotubes Improve Electrical Properties, Mechanical Adhesion, Neural Attachment, and Neurite Outgrowth of Neural Electrodes. *Small* **2010**, *6*, 421−429.
(30) Santos, M. I.; Tuzlakoglu, K.; Fuchs, S.; Gomes, M. E.; Peters, K.; Unger, R. E.; Piskin, E.; Reis, R. L.; Kirkpatrick, C. J. Endothelial Cell Colonization and Angiogenic Potential of Combined Nano- and Micro-Fibrous Scaffolds for Bone Tissue Engineering. *Biomaterials* **2008**, *29*, 4306−4313.
(31) Cheng, Z. A.; Zouani, O. F.; Glinel, K.; Jonas, A. M.; Durrieu, M.-C. Bioactive Chemical Nanopatterns Impact Human Mesenchymal Stem Cell Fate. *Nano Lett.* **2013**, *13*, 3923−3929.
(32) Bettinger, C. J.; Langer, R.; Borenstein, J. T. Engineering Substrate Topography at the Micro- and Nanoscale to Control Cell Function. *Angew. Chem., Int. Ed.* **2009**, *48*, 5406−5415.
(33) Karlsson, M.; Palsgard, E.; Wilshaw, P. R.; Di Silvio, L. Initial in Vitro Interaction of Osteoblasts with Nano-Porous Alumina. *Biomaterials* **2003**, *24*, 3039−3046.
(34) Chesnutt, B. M.; Yuan, Y.; Buddington, K.; Haggard, W. O.; Bumgardner, J. D. Composite Chitosan/Nano-Hydroxyapatite Scaffolds Induce Osteocalcin Production by Osteoblasts in Vitro and Support Bone Formation in Vivo. *Tissue Eng., Part A* **2009**, *15*, 2571−2579.
(35) Wang, Y.; Shi, H.; Qiao, J.; Tian, Y.; Wu, M.; Zhang, W.; Lin, Y.; Niu, Z.; Huang, Y. Electrospun Tubular Scaffold with Circumferentially Aligned Nanofibers for Regulating Smooth Muscle Cell Growth. *ACS Appl. Mater. Interfaces* **2014**, *6*, 2958−2962.
(36) Thapa, A.; Webster, T. J.; Haberstroh, K. M. Polymers with Nano-Dimensional Surface Features Enhance Bladder Smooth Muscle Cell Adhesion. *J. Biomed. Mater. Res., Part A* **2003**, *67*, 1374−1383.
(37) Dalby, M. J.; Riehle, M. O.; Sutherland, D. S.; Agheli, H.; Curtis, A. S. Changes in Fibroblast Morphology in Response to Nano-Columns Produced by Colloidal Lithography. *Biomaterials* **2004**, *25*, 5415−5422.
(38) Leszczak, V.; Smith, B. S.; Popat, K. C. Hemocompatibility of Polymeric Nanostructured Surfaces. *J. Biomater. Sci., Polym. Ed.* **2013**, *24*, 1529−1548.
(39) Smith, B. S.; Yoriya, S.; Grissom, L.; Grimes, C. A.; Popat, K. C. Hemocompatibility of Titania Nanotube Arrays. *J. Biomed. Mater. Res., Part A* **2010**, *95*, 350−360.
(40) Duling, R. R.; Lannutti, J.; Dupaix, R. B.; Katsube, N. Mechanical Characterization of Electrospun Polycaprolactone (PCL): A Potential Scaffold for Tissue Engineering. *J. Biomech. Eng.* **2008**, *130*, 011006−011006.
(41) Pektok, E.; Nottelet, B.; Tille, J. C.; Gurny, R.; Kalangos, A.; Moeller, M.; Walpoth, B. H. Degradation and Healing Characteristics of Small-Diameter Poly(epsilon-caprolactone) Vascular Grafts in the Rat Systemic Arterial Circulation. *Circulation* **2008**, *118*, 2563−2570.
(42) Leszczak, V.; Baskett, D.; Popat, K. Smooth Muscle Cell Functionality on Collagen Immobilized Polycaprolactone Nanowire Surfaces. *J. Funct. Biomater.* **2014**, *5*, 58−77.
(43) Popat, K. C.; Porter, J. R.; Henson, A. Biodegradable Poly(epsilon-caprolactone) Nanowires for Bone Tissue Engineering Applications. *Biomaterials* **2009**, *30*, 780−788.
(44) Zhu, Y.; Ong, W. F. Epithelium Regeneration on Collagen (IV) Grafted Polycaprolactone for Esophageal Tissue Engineering. *Mater. Science Eng., Part C* **2009**, *29*, 1046−1050.
(45) Cassie, A. Contact Angles. *Discuss. Faraday Soc.* **1948**, *3*, 11−16.
(46) Brash, J. L. Exploiting the Current Paradigm of Blood-Material Interactions for the Rational Design of Blood-Compatible Materials. *J. Biomater. Sci., Polym. Ed.* **2000**, *11*, 1135−1146.
(47) Smith, B. S.; Yoriya, S.; Grissom, L.; Grimes, C. A.; Popat, K. C. Hemocompatibility of Titania Nanotube Arrays. *J. Biomed. Mater. Res., Part A* **2010**, *95A*, 350−360.
(48) Woodruff, M. A.; Hutmacher, D. W. The Return of a Forgotten Polymer—Polycaprolactone in the 21st Century. *Prog. Polym. Sci.* **2010**, *35*, 1217−1256.
(49) Siegismund, D.; Schroeter, A.; Schuster, S.; Rettenmayr, M. Quantitative Modeling of Fibrinogen Adsorption on Different Biomaterials. *Cell Mol. Bioeng.* **2013**, *6*, 210−219.
(50) Nygren, H.; Alaeddin, S.; Lundström, I.; Magnusson, K.-E. Effect of Surface Wettability on Protein Adsorption and Lateral Diffusion. Analysis of Data and a Statistical Model. *Biophys. Chem.* **1994**, *49*, 263−272.
(51) Raffaini, G.; Ganazzoli, F. Understanding the Performance of Biomaterials through Molecular Modeling: Crossing the Bridge between Their Intrinsic Properties and the Surface Adsorption of Proteins. *Macromol. Biosci.* **2007**, *7*, 552−566.
(52) Lindon, J. N.; McManama, G.; Kushner, L.; Merrill, E. W.; Salzman, E. W. Does the Conformation of Adsorbed Fibrinogen Dictate Platelet Interactions with Artificial Surfaces? *Blood* **1986**, *68*, 355−362.
(53) Ogedegbe, H. O. An Overview of Hemostasis. *Lab Med.* **2002**, *33*, 948−953.

(54) Cerletti, C.; Tamburrelli, C.; Izzi, B.; Gianfagna, F.; de Gaetano, G. Platelet-Leukocyte Interactions in Thrombosis. *Thromb. Res.* **2012**, *129*, 263−266.
(55) Elstad, M. R.; McIntyre, T. M.; Prescott, S. M.; Zimmerman, G. A. The Interaction of Leukocytes with Platelets in Blood Coagulation. *Curr. Opin. Hematol.* **1995**, *2*, 47−54.
(56) Cerletti, C.; Tamburrelli, C.; Izzi, B.; Gianfagna, F.; de Gaetano, G. Platelet-Leukocyte Interactions in Thrombosis. *Thromb. Res.* **2012**, *129*, 263−266.
(57) Blezer, R.; Willems, G. M.; Cahalan, P. T.; Lindhout, T. Initiation and Propagation of Blood Coagulation at Artificial Surfaces Studied in a Capillary Flow Reactor. *Thromb. Haemostasis* **1998**, *79*, 296−301.
(58) Colman, R. W.; Schmaier, A. H. Contact System: A Vascular Biology Modulator with Anticoagulant, Profibrinolytic, Antiadhesive, and Proinflammatory Attributes. *Blood* **1997**, *90*, 3819−3843.
(59) Boon, G. D. An Overview of Hemostasis. *Toxicol. Pathol.* **1993**, *21*, 170−179.
(60) Sacks, S. H.; Chowdhury, P.; Zhou, W. Role of the Complement System in Rejection. *Curr. Opin. Immunol.* **2003**, *15*, 487−492.
(61) Vijayanand, K.; Pattanayak, D. K.; Mohan, T. R.; Banerjee, R. Interpreting Blood-Biomaterial Interactions from Surface Free Energy and Work of Adhesion. *Trends Biomater. Artif. Organs* **2005**, *18*, 73−83.